



Published in final edited form as:

Cell Rep. 2019 July 16; 28(3): 792–803.e4. doi:10.1016/j.celrep.2019.06.044.

Functional Inactivation of Mast Cells Enhances Subcutaneous Adipose Tissue Browning in Mice

Xian Zhang^{1,2,6}, Xin Wang^{1,6}, Hao Yin³, Lei Zhang¹, Airong Feng³, Qiu-Xia Zhang¹, Yan Lin¹, Bin Bao^{1,4}, Laura L. Hernandez⁵, Guo-Ping Shi^{1,2,7,*}, Jian Liu^{1,4,*}

¹School of Food and Biological Engineering, Hefei University of Technology, Hefei 230009, China

²Department of Medicine, Brigham and Women's Hospital and Harvard Medical School, Boston, MA 02115, USA

³Hefei National Laboratory for Physical Sciences at Microscale, University of Science and Technology of China, Hefei 230026, China

⁴Engineering Research Center of Bio-process, Ministry of Education, Hefei University of Technology, Hefei 230009, China

⁵Department of Dairy Science, University of Wisconsin, Madison, WI 53706, USA

⁶These authors contributed equally

⁷Lead Contact

SUMMARY

Adipose tissue browning and systemic energy expenditure provide a defense mechanism against obesity and associated metabolic diseases. In high-cholesterol Western diet-fed mice, mast cell (MC) inactivation ameliorates obesity and insulin resistance and improves the metabolic rate, but a direct role of adipose tissue MCs in thermogenesis and browning remains unproven. Here, we report that adrenoceptor agonist norepinephrine-stimulated metabolic rate and subcutaneous adipose tissue (SAT) browning are enhanced in MC-deficient *Kit^{w-sh/w-sh}* mice and MC-stabilized wild-type mice on a chow diet. MC reconstitution to SAT in *Kit^{w-sh/w-sh}* mice blocks these changes. Mechanistic studies demonstrate that MC inactivation elevates SAT platelet-derived growth factor receptor A (PDGFR α ⁺) adipocyte precursor proliferation and accelerates beige adipocyte differentiation. Using the tryptophan hydroxylase 1 (TPH1) inhibitor and TPH1-deficient MCs, we show that MC-derived serotonin inhibits SAT browning and systemic energy expenditure. Functional inactivation of MCs or inhibition of MC serotonin synthesis in SAT promotes adipocyte browning and systemic energy metabolism in mice.

*Correspondence: gshi@bwh.harvard.edu (G.-P.S.), liujian509@hfut.edu.cn (J.L.).

AUTHOR CONTRIBUTIONS X.Z. and X.W. conceived and designed the experiments, performed the study, and wrote the manuscript draft. H.Y., L.Z., A.F., Q.-X.Z., and Y.L. participated in the study and contributed to data analysis. B.B. contributed to data analysis and the manuscript draft. J.L. and G.-P.S. designed and funded the experiments and edited and finalized the manuscript.

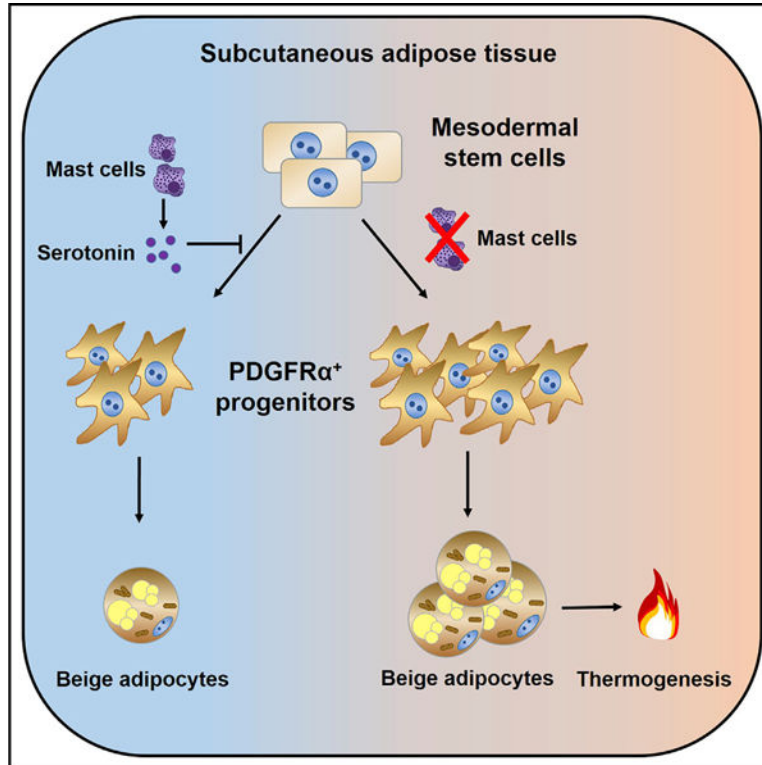
SUPPLEMENTAL INFORMATION

Supplemental Information can be found online at <https://doi.org/10.1016/j.celrep.2019.06.044>.

DECLARATION OF INTERESTS

The authors declare no competing interests.

Graphical Abstract



In Brief

Zhang et al. report that mast cell deficiency or pharmacological inhibition in mice increases subcutaneous adipose tissue (SAT) adipocyte browning and metabolic rate by increasing SAT PDGFR α ⁺ adipocyte precursor proliferation and beige adipocyte differentiation. Mechanistic analysis demonstrates that MC-derived serotonin inhibits SAT browning and systemic energy expenditure.

INTRODUCTION

Adipose tissue is a dynamic and plastic organ with profound effects on energy metabolism and nutritional homeostasis. Environmental, pharmacological, and nutritional stimuli affect adipose tissue metabolic phenotype and cellular composition (Rosen and Spiegelman, 2014). In humans and mice, adipocytes are grouped into unilocular white adipocytes and multilocular brown adipocytes (Cypess et al., 2009; Harms and Seale, 2013; Rosen and Spiegelman, 2014; Virtanen et al., 2009). White adipocytes are specialized to store chemical energy in the form of triglyceride, whereas brown adipocytes transform stored chemical energy into heat (Kajimura et al., 2015; Rosen and Spiegelman, 2014). Therapeutic targeting of brown adipocyte-mediated thermogenesis to increase energy expenditure may offer a viable approach to combat obesity and metabolic diseases (Harms and Seale, 2013; Kajimura and Saito, 2014).

Multiple lines of evidence indicate that there are two distinct types of UCP1 (uncoupled protein-1)-positive brown-like adipocytes: myogenic Myf5⁺ cellular lineage-derived classical brown adipocytes primarily in interscapular brown adipose tissue (BAT) deposits and Myf5⁻ PDGFR α ⁺ precursor-derived interspersed beige or brite cells within white adipose tissue (WAT) (Harms and Seale, 2013; Kajimura and Saito, 2014; Kajimura et al., 2015; Lee et al., 2012; Seale et al., 2008; Wu et al., 2012). Although external stimuli induce beige cell UCP1 expression, brown adipocytes are fat cell-autonomous for expression of high levels of UCP1 under non-stimulated conditions (Kajimura et al., 2015; Lee et al., 2012; Ohno et al., 2012; Wu et al., 2012). WAT bioenergetic analysis suggests that beige cells are bifunctionally suited for energy storage under basal conditions but fully capable of initiating heat production after receiving thermogenic stimuli or under loss of function of classic brown fat (Fisher et al., 2012; Wu et al., 2012). The bi-potential of PDGFR α ⁺ precursor differentiation into either the beige or white adipocyte lineage also depends on environmental signals (Lee et al., 2012). Secondary brown adipose tissue-mediated physiological networks, such as cross-talk between adipose tissue and skeletal muscle, liver, and immune cells, also control systemic energy homeostasis, which is independent of primary sympathetic nervous system control (Kajimura and Saito, 2014; Kajimura et al., 2015). This may explain how rapid thermogenic remodeling in poorly adrenergic nerve-innervated subcutaneous adipose tissue (SAT) is induced after exposure to peripheral stimuli. For instance, several endocrine factors from peripheral tissue, such as fibroblast growth factor 21 (FGF21) (Fisher et al., 2012) and bile acid (Watanabe et al., 2006) from liver, irisin (Boström et al., 2012), meteorin-like (Rao et al., 2014), and transforming growth factor β (TGF- β) (Yadav et al., 2011) from skeletal muscle regulate brown or beige fat development and thermogenesis and mediate interorgan communication with the central and peripheral tissues. In addition, ILC2 (type 2 innate lymphoid cells)- and eosinophil-derived interleukin-4 (IL-4) and IL-13 stimulate proliferation of PDGFR α ⁺ precursors and induce catecholamine production from alternatively activated macrophages to promote beige fat biogenesis (Lee et al., 2015; Qiu et al., 2014). Our previous study showed that genetic deficiency and pharmacological stabilization of mast cells (MCs) increased the metabolic rate and UCP1 expression in brown adipocytes in Western diet-fed mice in concert with obesity and insulin resistance improvement (Liu et al., 2009). However, it remains unknown whether MCs play a direct role in energy homeostasis or whether the aforementioned changes in energy expenditure are merely secondary to mouse body weight reduction.

Here we report that genetic deficiency and stabilization of MCs activate a thermogenic program and stimulate beige fat biogenesis in SAT and that adoptive transfer of MCs to recipient mouse SAT reverses these changes. We also show that MCs decrease SAT PDGFR α ⁺ beige precursor cells and inhibit SAT adipocyte browning differentiation. This activity of MCs depends on MC-derived serotonin, providing fundamental insights into how MCs affect WAT beige adipocyte commitment and thermogenesis.

RESULTS

MC Functional Inactivation Activated Systemic Energy Expenditure and SAT Thermogenesis and Browning in Mice

To assess direct participation of MCs in energy homeostasis, we compared metabolic differences between wild-type (WT) and MC-deficient *Kit^{w-sh/w-sh}* mice. In the context of mice on a chow diet, there were no differences in their body weight (Figure S1A) and energy intake (Figure S1B). However, administration of an adrenoceptor agonist, norepinephrine (NE) (Lim et al., 2012), ended *Kit^{w-sh/w-sh}* mice with higher oxygen consumption (Figure 1A), carbon dioxide production (Figure 1B), and body temperature (Figure 1C) than WT mice. Similarly, WT mice receiving daily treatment with an MC stabilizer, disodium cromoglycate (DSCG) (Liu et al., 2009), also showed an increased metabolic rate (Figures 1A–1C), although their body weight and food intake were comparable with those of saline-treated WT mice (Figures S1A and S1B). These observations suggest an association between MCs and energy expenditure.

Because brown and beige adipocytes are specialized in energy expenditure through thermogenesis (Kajimura and Saito, 2014; Kajimura et al., 2015; Rosen and Spiegelman, 2014; Wu et al., 2012), we examined the expression of thermogenic marker UCP1 in adipose tissues in these mice. H&E (Figure S2A) and UCP1 immunohistochemical (Figure 1D) staining revealed more multilocular UCP1⁺ beige cells in SAT from *Kit^{w-sh/w-sh}* mice and DSCG-treated WT mice compared with control mice, although such a difference did not appear in either BAT or epididymal adipose tissue (EAT) from the same groups of mice (Figures S2A and S2B). A western blot with a polyclonal antibody against UCP1 supported these histological results (Figure 1E; Figures S3A and S3B), although BAT expressed significantly more UCP1 than EAT and SAT (Figure S3B). SAT (Figure 1F) from *Kit^{w-sh/w-sh}* mice and DSCG-treated WT mice also contained much higher mRNA levels of *Ucp1* and other thermogenic and mitochondrial genes, including *Pgc1 α* , *Prdm16*, *Cidea*, *Elovl3*, *Ndufv2*, and *Ndufb5*, compared with SAT from the corresponding control mice. However, MC deficiency or inhibition with DSCG did not affect most of these genes in EAT (Figure S3C) or BAT (Figure S3D). DSCG only increased EAT expression of *Cidea* (cell death-inducing DNA fragmentation factor alpha-like effector A), which controls adipose tissue macrophage accumulation and insulin sensitivity (Abreu-Vieira et al., 2015), and MC deficiency increased the expression of *Pgc1 α* (peroxisome proliferator-activated receptor γ coactivator 1 α), which regulates BAT thermogenesis (Wu et al., 1999; Uldry et al., 2006). These changes in EAT and BAT may also contribute to the enhanced metabolic rate in *Kit^{w-sh/w-sh}* mice and DSCG-treated WT mice (Figures 1A–1C). Therefore, functional inactivation of MCs, including genetic deficiency and pharmacological stabilization, may increase systemic energy expenditure by inducing SAT browning and thermogenesis.

MC Reconstitution in SAT Reversed the Systemic Energy Metabolism and SAT Browning in *Kit^{w-sh/w-sh}* Mice

To further evaluate the effects of MCs on adipose tissue thermogenesis, we performed toluidine blue staining to detect MC numbers in various adipose tissues. In WT mice, SAT contained many more MCs than EAT or BAT (Figures S4A and S4B), which was supported

by higher mRNA levels of the MC markers (Caughey, 2011) *mMcp-4* (Figure S4C) and *mMcp-6* (Figure S4D) in SAT compared with those in EAT or BAT. Consistent with our prior report (Liu et al., 2009), DSCG as an MC stabilizer reduced MC degranulation but did not change MC numbers in adipose tissues (Figures S4E and S4F). Fluorescence-activated cell sorting (FACS) analysis quantified the number of FcεR1⁺CD117⁺ MCs in different adipose tissues and also showed that MCs were enriched in SAT compared with EAT and BAT (Figure S4G). DSCG treatment also did not change their numbers in any of these adipose tissues. To test for a role of MCs in suppressing the thermogenic program in SAT and in reducing the mouse metabolic rate, we prepared bone marrow-derived MCs (BMMCs) from WT mice and transferred these cells into *Kit^{w-sh/w-sh}* mice using three injection approaches, including intravenous (i.v.), intraperitoneal (i.p.), and subcutaneous (s.c.) injections, respectively. 6 weeks after BMMC adoptive transfer, only the s.c. injection approach (Figures 2A and 2B), but not the i.v. (Figures 2C and 2D) or i.p. (Figures 2E and 2F) injection approaches, significantly decreased the NE-stimulated metabolic rate in *Kit^{w-sh/w-sh}* recipient mice. *Kit^{w-sh/w-sh}* mice receiving BMMCs by s.c. injection also showed a lower body temperature than saline-treated controls (Figure 2G). Immunohistochemistry (Figure 2H) and immunoblot (Figure 2I) for UCP1 and real-time PCR analysis for thermogenic and mitochondrion-related genes (Figure 2J) supported the conclusion that s.c. BMMC reconstitution reversed the MC deficiency-induced enhancements of SAT browning and thermogenesis. Such changes diminished in *Kit^{w-sh/w-sh}* mice receiving i.v. or i.p. BMMC reconstitution (Figures 2H, 2I, S5A, and S5B). These observations suggested that s.c. injection of BMMCs was a better approach than the i.v. or i.p. approach to reconstitute MCs into SAT and to reverse the thermogenic program in *Kit^{w-sh/w-sh}* mice. Toluidine blue staining of MCs supported this conclusion. *Kit^{w-sh/w-sh}* mice receiving s.c. BMMC injections had many more MCs in SAT than those that received i.v. or i.p. BMMC injections (Figures 2K and 2L). FACS analysis demonstrated that these donor BMMCs from s.c. injections went to the SAT but negligibly to the EAT (Figure S5C). Together, these results support the hypothesis that SAT MCs suppress local adipocyte browning and thermogenesis and reduce systemic energy expenditure.

MCs Inhibited SAT PDGFRα⁺ Beige Progenitor Cell Proliferation and Browning

PDGFRα⁺ cells are bipotential adipocyte progenitors and capable to differentiate into either white or beige adipocytes (Lee et al., 2012). We investigated the cellular origins of nascent SAT beige adipocytes induced by MC functional inactivation. Real-time PCR analysis of SAT revealed that both *Kit^{w-sh/w-sh}* and DSCG-treated mice had higher expression of the beige cell markers *CD137*, *Tmem26*, *Tbx1*, *Cited1*, and *Shox2* and the beige progenitor marker *Pdgfra* as well as the pre-adipocyte markers *AEBP1* and *GATA2* (Chlon and Crispino, 2012; He et al., 1995) than their corresponding controls (Figure 3A). FACS analysis also demonstrated that MC deficiency or inhibition significantly elevated the percentage of CD34⁺PDGFRα⁺ cells in the SAT stromal vascular fraction (SVF) (Figure 3B). Immunofluorescence analysis revealed many more PDGFRα⁺ cells in SAT from *Kit^{w-sh/w-sh}* and DSCG-treated mice compared with control mice, and many of these PDGFRα⁺ cells also expressed UCP1 (Figure 3C). Ki67 and PDGFRα immunofluorescent double staining showed that the numbers of Ki67⁺PDGFRα⁺ proliferating progenitors in SAT from *Kit^{w-sh/w-sh}* and DSCG-treated mice were increased compared with control mice

(Figure 3D). Therefore, functional inactivation of MCs stimulated beige fat biogenesis in SAT by enhancing browning differentiation and PDGFR α ⁺ adipocyte progenitor proliferation.

To assess a direct role of MCs in interfering SAT adipocyte beiging or PDGFR α ⁺ adipocyte progenitor browning, we isolated fresh SVF from SAT from WT mice and incubated it with live BMMCs or a BMMC lysate preparation for 6 days without the browning differentiation cocktail. Live BMMCs or the BMMC lysate preparation inhibited expression of the SVF beige progenitor marker *Pdgfra* from these SVF preadipocytes (Figure 4A). In an independent study, SVF was induced for browning differentiation for 8 days. The presence of live BMMCs or the BMMC lysate preparation suppressed the expression of thermogenic genes in these differentiated SVF adipocytes (Figure 4B), although neither live BMMCs nor the BMMC lysate affected SAT SVF preadipocyte adipogenesis (Figure S6). We made the same observations in cultured SAT explants. Live BMMCs or the BMMC lysate preparation also reduced expression of the same set of thermogenic genes from the SAT explants (Figure 4C). Adipose tissue is a major site for cholesterol storage (Krause and Hartman, 1984; Kovanen et al., 1975), which activates MCs much more potently than immunoglobulin E (IgE) (Zhang et al., 2019). Cell culture medium from low-density lipoprotein (LDL)-activated BMMCs, but not that from non-activated BMMCs, acted the same as live BMMCs or BMMC lysate in suppressing thermogenic gene expression in *in vitro* browning-differentiated SVF adipocytes (Figure 4B). These findings demonstrate direct participation of MCs in inhibiting the thermogenic program in SAT SVF. This inhibitory effect of BMMCs is induced after BMMC activation and independent of cell-cell contact.

MC-Derived Serotonin Inhibited Systemic Energy Expenditure and the SAT Thermogenic Program

Serotonin, an important regulator of energy balance (Berglund et al., 2013; Crane et al., 2015; Oh et al., 2015; Tecott, 2007), is synthesized and released from central or peripheral cells, such as raphe neurons, pinealocytes, MCs, and intestinal and pancreatic enterochromaffin cells (Gershon and Ross, 1966). Peripheral serotonin is synthesized from tryptophan by tryptophan hydroxylase 1 (TPH1) and can directly suppress *Ucp1* expression in BAT and in brown and beige adipocytes (Crane et al., 2015). To identify the mediator from MCs that regulated adipocyte browning and thermogenesis in SAT, we assessed the expression of TPH1 in SAT from different groups of mice by real-time PCR. TPH1 expression was greatly suppressed in SAT from *Kit^{w-sh/w-sh}* mice and those receiving DSCG treatment but partially reversed in *Kit^{w-sh/w-sh}* mice after receiving BMMC s.c. reconstitution (Figure 5A). Ultra-fast liquid chromatography and tandem mass spectrometry (UPLC-MS/MS) allowed detection of SAT serotonin levels. In WT mice, the SAT serotonin level was 18.5 ± 6 ng/g, comparable with that from a previous report (Stock and Westermann, 1963). However, serotonin was undetectable in SAT from *Kit^{w-sh/w-sh}* mice and significantly reduced in SAT from DSCG-treated WT mice (Figure 5B). *Kit^{w-sh/w-sh}* mice receiving s.c. injections of BMMCs had SAT serotonin levels similar to those from WT mice (Figure 5B). To identify the sources of SAT serotonin production, we isolated adipocytes, SVF, MCs, and MC-free SVF from SAT from WT mice. TPH1 expression in the SVF or purified MCs was significantly higher than in adipocytes, and it was sharply reduced

after MCs were removed from the SVF (Figure 5C). Immunofluorescent double staining colocalized TPH1 expression to CD117⁺ MCs in SAT (Figure 5D). Immunoblot and real-time PCR detected TPH1 expression in cultured BMMCs but negligible expression in 3T3-L1 preadipocytes or differentiated 3T3-L1 adipocytes (Figures 5E and 5F). MC activation with LDL induced BMMC TPH1 expression that was blunted by the TPH1 inhibitor LX1031 (Figure 5G).

An adipocyte differentiation cocktail promotes SVF preadipocyte differentiation into adipocytes (Shan et al., 2013). ELISA detected negligible serotonin in the culture medium from SVF preadipocytes or adipocytes compared with that from BMMCs. After 48 h of treatment, the MC activator LDL increased BMMC serotonin release but did not affect SVF adipocyte serotonin production. The TPH1 inhibitor LX1031 dose-dependently reduced LDL-induced BMMC serotonin secretion (Figure 5H). Real-time PCR revealed the same patterns of TPH1 expression in SVF preadipocytes, adipocytes, and BMMCs treated with or without LDL or LX1032 (Figure 5I). All of these observations from different approaches, including immunoblot, immunofluorescent staining, and real-time PCR, proved that SAT MCs, but not adipocytes or pre-adipocytes, are the major source of TPH1 and serotonin in SAT.

To further investigate a role of MC TPH1 in SAT serotonin production and systemic energy expenditure, we gave *Kit^{w-sh/w-sh}* mice that received s.c. adoptive transfer of WT BMMCs a peripheral TPH1 inhibitor, LX1031, that should not affect central serotonin synthesis (Camilleri, 2011). As expected, LX1031 treatment lowered TPH1 expression (Figure 5A) and serotonin release (Figure 5B) in SAT from BMMC-reconstituted *Kit^{w-sh/w-sh}* mice, as determined by real-time PCR and UPLC-MS/MS, respectively. Although LX1031 treatment did not affect MC repopulation in recipient mouse SAT (Figures S7A and S7B), this TPH1 inhibitor greatly increased mouse NE-induced oxygen consumption (Figure 6A) and carbon dioxide production (Figure 6B). LX1031 also increased the numbers of UCP1⁺ beige adipocytes (Figure 6C) and UCP1⁺PDGFR α ⁺ beige progenitors (Figure 6D) in SAT from s.c. BMMC-reconstituted *Kit^{w-sh/w-sh}* mice. Congruently, immunoblotting and real-time PCR demonstrated that TPH1 inhibition by LX1031 increased the UCP1 protein (Figure 6E) and mRNA levels of the thermogenic genes *Ucp1*, *Cidea*, and *Elovl3* (Figure 6F); the beige adipocyte markers *CD137*, *Tmem26*, and *Cited1* (Figure 6G); and the beige progenitor marker *Pdgfra* (Figure 6H) in SAT from s.c. BMMC-reconstituted *Kit^{w-sh/w-sh}* mice.

Adoptive transfer of BMMCs from TPH1-deficient *Tph1^{-/-}* mice to *Kit^{w-sh/w-sh}* recipient mice yielded the same results. Relative to those receiving adoptive transfer of WT BMMCs by s.c. injection, *Kit^{w-sh/w-sh}* recipient mice receiving BMMCs from *Tph1^{-/-}* mice demonstrated significant recovery of UCP1 protein or mRNA levels, as determined by immunostaining (Figure S8A), immunoblot analysis (Figure S8B), and real-time PCR (Figure S8C). SAT from *Kit^{w-sh/w-sh}* mice receiving *Tph1^{-/-}* BMMCs also showed significantly higher mRNA levels of thermogenic genes (Figure S8C), beige cell markers, and the beige progenitor marker *Pdgfra* (Figure S8D) than those receiving WT BMMCs.

DISCUSSION

Brown and beige adipose tissues take in glucose and lipids from the circulation and act as important metabolically active organs (Loyd and Obici, 2014). Brown and beige adipocytes play important roles in glucose homeostasis, insulin sensitivity, lipid metabolism, and energy expenditure, all of which are key elements in the pathogenesis of obesity and diabetes (Ghorbani et al., 1997; Harms and Seale, 2013; Stanford et al., 2013). Adipocyte beiging helps to control body weight gain and maintain glucose and lipid homeostasis (Kaisanlahti and Glumoff, 2019; Mössenböck et al., 2014). We reported previously that adipose tissue MCs play a pathogenic role in western diet-induced obesity and diabetes by releasing pro-inflammatory cytokines (Liu et al., 2009). This study revealed a previously untested inhibitory function of MCs in SAT browning in mice fed a chow diet. MCs in SAT from these mice suppressed local adipocyte browning, thermogenesis, and population expansion of PDGFR⁺ beige progenitors, an important source of beiging cells in mouse SAT or in SAT SVF *ex vivo*. Using the THP1 inhibitor LX1031 and MCs from *Tph1*^{-/-} mice, we demonstrated that MC serotonin was responsible for these MC activities. Functional inactivation of MCs, including genetic deficiency and pharmacological stabilization, increased systemic energy expenditure by enhancing SAT adipocyte browning and thermogenesis. Therefore, targeting MC serotonin to increase SAT beige adipocyte formation may become a potential therapeutic strategy to treat obesity and type 2 diabetes.

Physiological stimuli such as cold exposure or caloric restriction may promote adipocyte browning through type 2 immune signaling (Fabbiano et al., 2016; Qiu et al., 2014). Several immune signaling-regulated beige fat thermogenic circuits have been established in adipose tissues, including type 2 immune signaling from ILC2s and eosinophils and their type 2 cytokines IL-4 and IL-13 (Brestoff et al., 2015; Fabbiano et al., 2016; Lee et al., 2015; Qiu et al., 2014); the IL-4-stimulated, alternatively activated macrophage axis (Nguyen et al., 2011); adipose-resident invariant natural killer T (iNKT) cell-induced FGF21 (Lynch et al., 2016); T cell-specific Stat6/Pten axis-linked Foxp3⁺ regulatory T (Treg) cell induction (Kalin et al., 2017); and $\gamma\delta$ T cell-derived IL-17A suppressing age-dependent ST2⁺ Treg and IL-33 abundance (Kohlgruber et al., 2018). Therefore, not only MCs, but also other immune cells affect the thermogenic program in SAT. It is possible that MCs may interact with these inflammatory cells and indirectly affect the immune signals in SAT thermogenesis regulation, although this study did not test this hypothesis. The interactions between MCs and macrophages (Liu et al., 2009; Zhou et al., 2015), Treg cells (Gri et al., 2008; Piconese et al., 2009), and ILC2s (Burton et al., 2018) suggest the possibility of such crosstalk when considering MC effects on thermogenesis.

MCs are commonly activated by IgE-antigen cross-linking, which results in release of preformed molecules, including histamine, serotonin, tryptase, chymase, and lipid-derived mediators, from the granules as well as by IgE-independent non-allergic responses that release both preformed and newly synthesized MC mediators, including cytokines and chemokines (Kalesnikoff and Galli, 2008). Adipose tissue is the major organ of cholesterol storage (Krause and Hartman, 1984; Kovanen et al., 1975). In SAT from chow diet-fed mice, there is about 150 g of cholesterol per gram of SAT. LDL at 1 mg/mL showed a similar potency of MC activation as 50 μ g/mL of IgE antibody (Zhang et al., 2019). Although we

did not quantitate the IgE content in SAT, plasma IgE levels from chow diet-fed mice reached about 100 ng/mL (Wang et al., 2011). Therefore, it is possible that cholesterol may be the major MC activator in SAT. Here we showed that activation of BMDCs with 1 mg/mL of LDL increased TPH1 mRNA levels by ~10-fold and the TPH1 protein level and serotonin level by ~2-fold. In addition to serotonin, histamine, prostaglandin, and IL-6 have been implicated in energy expenditure regulation (García-Alonso et al., 2016; Karlstedt et al., 2003; Knudsen et al., 2014; Sakata et al., 1995). MCs in adipose tissues may also release these mediators to act similarly as serotonin. Therefore, targeting MC serotonin, and possibly histamine, prostaglandin, IL-6, or other untested mediators, in adipose tissue may help boost the fat tissue-specific adipocyte browning mechanism and energy expenditure without affecting MC activities in other organs.

Results from Kit-dependent, MC-deficient *Kit^{w-sh/w-sh}* mice may be confounded by changes in other immune cells (Nigrovic et al., 2008). It is essential to use the MC reconstitution approach to verify the role of MCs in studies using these mice (Liu et al., 2009). Use of MC inhibitors would provide another line of evidence to support MC function (Liu et al., 2009). It has also been commented that donor MCs, after adoptive transfer, may show potential differences in number recovery and anatomical distribution in recipient mice. Therefore, donor MCs may never act the same as native endogenous MCs (Rodewald and Feyerabend, 2012; Gutierrez et al., 2015). In this study, however, we used several approaches to prove a role of MCs in dysregulating SAT adipocyte browning and systemic energy expenditure, including use of the MC inhibitor DSCG, adoptive transfer of MCs from WT and *Tph1^{-/-}* mice, treatment of MC chimeric mice with and without the TPH1 inhibitor LX1031, and the s.c. injection approach to deliver donor MCs to SAT. Nevertheless, the effect of altered immune cells in *Kit^{w-sh/w-sh}* mice may still present. Therefore, use of kit-independent MC-deficient mice without affecting other immune cells (Gutierrez et al., 2015) may further support our conclusion.

FACS analysis allowed quantification of SAT MC content. We detected about 1,000 MCs per gram of SAT from WT mice, but there were only about 160 MCs per gram of SAT from *Kit^{w-sh/w-sh}* mice after receiving s.c. adoptive transfer of 3×10^6 donor BMDCs. However, decreases in metabolic rate, body temperature, SAT expression of UCP1, and thermogenic genes all reached statistical significance. Although we cannot explain why such a low number of donor MCs in SAT nearly completely reversed these metabolic parameters to the levels in WT mice, our prior study of Western diet-induced obesity and diabetes revealed similar changes. About 50% re-population of WAT MCs in *Kit^{w-sh/w-sh}* mice receiving 1.3×10^7 donor BMDCs by i.v. adoptive transfer yielded levels of obesity and diabetes comparable with those of WT control mice (Liu et al., 2009), supporting the importance of WAT MCs in the thermogenic program and systemic energy expenditure. It also remains unexplained why MC stabilization with DSCG did not affect MC numbers in SAT, EAT, or BAT but reduced the expression of TPH1 and consequent production of serotonin. It is possible that blockage of MC degranulation led to intracellular accumulation of serotonin, which may suppress its synthesis as a feedback mechanism, although we did not test this hypothesis in this study.

Our earlier study used the same *Kit^{w-sh/w-sh}* mice and the MC inhibitor DSCG and demonstrated a role of MCs in Western diet-induced obesity and diabetes. MC deficiency or inhibition with DSCG reduced UCP1 expression in BAT when mice were on a Western diet (Liu et al., 2009). In SAT from *Kit^{w-sh/w-sh}* mice, however, we detected significantly higher levels of the thermogenic and mitochondrial genes *Pgc1a*, *Prdm16*, *Cidea*, *Elovl3*, and *Ndufv2* and the beige cell markers *CD137* and *Tmem26* compared with SAT from WT mice when mice were on a chow diet or a Western diet (data not shown). When mice were induced to develop obesity and diabetes, MC distribution in adipose tissue may differ from that in mice on a chow diet. Therefore, MC activity and distribution may change depending on the types of environmental, pharmacological, and nutritional stimuli. Together, the observations from this study suggest that MCs in SAT maintain thermogenesis at the basal level when mice consume a chow diet. Functional inactivation of MCs by genetic deficiency or pharmacological inhibition (e.g., DSCG) increases SAT adipocyte browning and thermogenesis and enhances systemic energy expenditure.

STAR*METHODS

LEAD CONTACT AND MATERIALS AVAILABILITY

Further information and requests for resources and reagents should be directed to the Lead Contact Guo-Ping Shi, DSc. (gshi@bwh.harvard.edu).

EXPERIMENTAL MODEL AND SUBJECT DETAILS

Mice—Wild-type (C57BL/6J) were from Vital River Laboratory Animal Technology Co. Ltd. (Beijing, China) and *Kit^{w-sh/w-sh}* (C57BL/6J) mice were from the Jackson Laboratories (Bar Harbor, ME, USA). *Tph1^{-/-}* mice were reported previously (Laporta et al., 2014). All animal procedures were approved by the Hefei University of Technology Standing Committee on Animals. To stimulate thermogenesis, 12-week-old mice were injected with norepinephrine (Sigma-Aldrich, St. Louis, MO) as previously reported (Lim et al., 2012).

Experimental animals and indirect calorimetry—Mice were housed and bred in ventilated cages within a pathogen-free barrier facility. Only male mice were used in this study. To stabilize MCs, 8-week-old WT mice were injected daily with DSCG (25 mg kg⁻¹ bodyweight, Sigma-Aldrich) for 4 weeks as previously described (Liu et al., 2009). For BMMC reconstitutions, 6-week-old *Kit^{w-sh/w-sh}* mice were subcutaneously injected with 3×10⁶ WT or *Tph1^{+/+}* BMMCs (Thevenot et al., 2011), intraperitoneally injected with 1×10⁶ WT BMMCs (Mallen-St Clair et al., 2004; Wolters et al., 2005) or injected via tail vein with 1×10⁷ WT BMMCs (Liu et al., 2009) for 6 weeks. To inhibit serotonin synthesis, 6-week-old *Kit^{w-sh/w-sh}* mice received subcutaneous BMMC reconstitution were given a daily subcutaneous injection of the TPH1 inhibitor LX1031 (10 mg kg⁻¹ bodyweight, Medchem Express, Monmouth Junction, NJ) for 6 weeks (Camilleri, 2011). At the end of each course of treatment, mouse bodyweight, core body temperature, and indirect calorimetry were measured and then mice were euthanized by CO₂ narcosis.

Norepinephrine (NE)-induced metabolic parameters, including whole body oxygen consumption rates and carbon dioxide production rates, were continuously monitored using

a combined indirect calorimetry system (TSE Systems, Inc., Chesterfield, MO). In brief, mice were anesthetized by intraperitoneal injection of 40–60 mg/kg pentobarbital, and transfer each mouse into a single metabolic chamber to measure the basic metabolic rate for 30 min without interruption. Then, open the metabolic chamber to inject 1 mg/kg NE into each mouse subcutaneous dorsal, and continue to measure metabolic rate for another 1 hour. Core body temperatures were measured rectally using a themocoupler (Physitemp Instruments, Inc., Clifton, NJ).

Cell culture—SVF and adipocytes were fractioned from SAT in WT or *Kit^{w-sh/w-sh}* mice as described (Zhang et al., 2016). To detect beige progenitors in SVF, SVF was separated on the basis of cell-surface markers using a flow cytometer MoFlo XDP (Beckman Coulter, Brea, CA). To remove MC from SVF from SAT, MCs were stained and sorted with MC-specific antibodies.

BMMCs and BMMC lysates were prepared from bone marrow cells in WT mice as previously reported (Liu et al., 2009). To assess the direct effect of MCs on *Pdgfra* expression in SVF, SVF was co-cultured in DMEM medium together with live BMMCs (1×10^5 per well for 24-well plate) or BMMC lysates (equivalent to the live cell numbers) for 6 days. To induce SVF browning differentiation, SVF was cultured in browning differentiation medium for 8 days and the differentiated adipocytes were stained by Oil-red O (Sigma-Aldrich) as previously reported (Zhang et al., 2014). During the 8 days of browning differentiation, live BMMCs, BMMC lysates, or culture media from non-activated or LDL-activated BMMCs were added to examine the effect of MCs on SVF browning differentiation. SAT explants were harvested from *Kit^{w-sh/w-sh}* mice and co-cultured with BMMCs or lysates for 24 hr as previously described (Du et al., 2011).

WAT SVF and adipocyte fractionation—Primary stromal vascular fraction (SVF) and adipocytes were fractioned from SAT from 8–16 weeks old WT or *Kit^{w-sh/w-sh}* mice. Briefly, adipose tissues were minced and digested with type II collagenase (2 mg/ml) in Krebs-Ringer bicarbonate *buffer* containing 10 mM HEPES (pH7.4) and 5% FBS for 30 min at 37 C. After removing non-digested tissues, suspended adipocytes and SVF were separated by passing through a 200 mesh strainer. SVF was incubated in red blood cell lysis buffer for 5 min at room temperature, and then, the cells were collected by centrifugation at 200 g for 10 min. Adipocytes were used for real time-PCR (RT-PCR) and SVF was prepared for RT-PCR, flow cytometry, and browning differentiation.

Cell and organ cultures—BMMCs were induced from bone marrow from 8-week-old mice. Bone marrow single cell preparations were cultured in RPMI 1640 medium containing 10 ng/ml murine recombinant IL-3 for 2 weeks and then in IL-3 and 50 ng/mL murine recombinant stem cell factor (PeproTech, New Jersey, USA) for another 3 weeks. After 5 weeks, cell purity was confirmed by FACS to show the cell surface expression of FcεRI and CD117 (> 98%). To activate BMMCs, BMMCs were treated with 1 mg/mL LDL (Lee Biosolutions, Inc, Mary-land Heights, MO) for 48 hr as previously described (Zhang et al., 2019) with or without 1 μM, 10 mM or 50 μM of LX1031.

Primary SVF from SAT was cultured in DMEM supplemented with 10% FBS and 1% penicillin/streptomycin and murine preadipocytes 3T3-L1 (ATCC, Manassas, VA) were cultured in DMEM containing 10% calf serum and 1% penicillin/streptomycin.

For SVF browning differentiation, confluent cells were cultured in DMEM medium supplemented with 850 nM insulin, 0.5 mM isobutylmethylxanthine, 1 μ M dexamethasone, 125 nM indomethacin, 1 nM 3,3',5-triiodo-L-thyronine (T3) and 1 μ M rosiglitazone (all from Sigma-Aldrich) for 2 days. Cells were then cultured in DMEM medium supplemented with insulin, T3, and rosiglitazone for another 6 days. SVF preparations on 24-well plate were also treated with 1×10^5 per well BMMC lysates, 1×10^5 per well live BMMCs, or culture media from LDL-activated or non-activated equivalent BMMCs at the beginning of brown adipocyte differentiation.

For SAT SVF and 3T3-L1 adipocyte differentiation, confluent cells were cultured in DMEM supplemented with 10% FBS, 850 nM insulin, 0.5 mM isobutylmethylxanthine, and 1 μ M dexamethasone (all from Sigma-Aldrich) for 2 days, and then in DMEM supplemented with 10% FBS and insulin for another 6 days. After differentiation, 1 mg/mL LDL was also added to fully differentiated adipocytes for 48 hr.

For adipocyte Oil-red O staining, after 8 days of browning differentiation, SVF was washed once with PBS and fixed with 4% paraformaldehyde for 1 hour, followed by incubation with Oil-red O (Sigma-Aldrich) for 4 hours.

To culture SAT tissue explants with BMMCs, SAT from 12-week-old *K_{it}^{w-sh/w-sh}* mice was isolated and cut into ~10 mg size pieces, then rinsed three times with PBS. Two pieces of SAT tissue in each well on a 24-well plate were co-cultured with or without 1×10^5 live BMMCs or equivalent lysates for 24 hr in DMEM supplemented with 10% FBS and 1% penicillin/streptomycin.

METHOD DETAILS

Real-time PCR, western blot, and histological study—For real-time PCR analysis, total RNA was extracted from adipose tissues or cells as described (Zhang et al., 2016). All primer sequences used in this study were listed in Table S1. Adipose tissue proteins were extracted and used for immunoblot analysis as previous reported (Liu et al., 2009). Adipose tissues were harvested and paraffin sections prepared for histological analysis.

Serotonin measurement—The level of serotonin in SAT was determined by UPLC-MS/MS (Thermo Fisher Scientific, Accela 600pump UPLC system equipped with LTQ Orbitrap XL mass spectrometer) as described previously with some modifications (He et al., 2013). Briefly, SAT were weighed and homogenized in a 20-fold (w/v) volume of 0.2% formic acid (v/v) in methanol. After centrifugation at 12,000 g for 30 min at 4 C, the supernatants were stored at 80 C until detection. Serotonin levels in cell culture medium were detected using mouse ELISA kits according to manufacturer protocols (LDN, Nordhorn, Germany).

Flow Cytometry—Primary SVF from EAT, SAT, BAT was resuspended in PBS with 2% FBS, and incubated with FACS antibodies for 30 min on ice. Cells were initially selected by size on the basis of forward scatter (FSC) and side scatter (SSC), following separated on the basis of cell-surface markers using a flow cytometer MoFlo XDP (Beckman Coulter, Brea, CA). To detect beige progenitors in SVF, primary SVF was separated on the basis of cell-surface markers including anti-PDGFR α (CD140a)-APC (1:50, BioLegend, San Diego, CA) and anti-CD34-FITC (1:100, eBioscience, San Diego, CA). To quantify MCs in adipose tissues, to isolate MCs from SVF, and to remove MCs from SVF, we stained and sorted MCs with anti-CD34-FITC (1:100, eBioscience), anti-CD45-PE (1:500, eBioscience) and MC markers anti-CD117-APC (1:200, eBioscience) and anti-FC ϵ R1-PE-CY7 (1:200, eBioscience). The MC-removed SVF and MCs (1×10^5) were collected for TPH1 mRNA expressional analysis.

Histology and immunohistochemistry—Adipose tissues were fixed in 4% formalin, embedded in paraffin and serially sliced into 7 mm thickness. To detect adipocyte morphology, MCs, and UCP1⁺ cells, adipose tissue paraffin sections were stained with hematoxylin-eosin (Sigma-Aldrich), toluidine blue (Sigma-Aldrich), or rabbit anti-UCP1 antibody (1:500, Abcam, Cambridge, MA) according to the standard protocols, respectively. For Immunofluorescence analysis, goat anti-PDGFR α (1:500, R&D Systems, Inc., Minneapolis, MN), rabbit anti-UCP1 (1:500, Abcam), rabbit anti-TPH1 (1:50, Millipore, Bedford, MA); rat anti-CD117 (1:50, ebioscience) and rabbit anti-Ki67 (1:100, Novus, Centennial, CO) antibodies were used as primary antibodies. For Immunofluorescence co-localization analysis, adipose tissues paraffin sections were sequentially stained with goat anti-PDGFR α and rabbit anti-UCP1; anti-PDGFR α and rabbit anti-Ki67, or rabbit anti-TPH1 and rat anti-CD117 antibodies according to the standard protocols (Kumar et al., 1999; Würden and Homberg, 1993). Slides were counterstained with DAPI (1:100, Sangon Biotech Co. Ltd., Shanghai, China).

Total RNA isolation and quantitative real-time PCR—Total RNA was extracted from adipose tissues using RNAiso Plus reagent (TAKARA, Dalian, China), and then reverse transcribed to cDNA using oligo d(T)₁₈ (TAKARA) and M-MLV reverse transcriptase (Invitrogen, Carlsbad, CA) according to manufacturer's protocol. Real-time PCR was analyzed using SYBR green dye (TAKARA) in a Bio-Rad MyiQ2 Real-time PCR System. Data were processed using the DDCT method when β -actin was used as the reference gene.

Immunoblot analysis—Tissue or cell proteins were extracted using the RIPA lysis buffer (50 mM Tris HCl, pH 7.4, 150 mM NaCl, 1% NP-40, 0.5% sodium deoxycholate, 0.1% SDS) containing protease and phosphatase inhibitors (Sangon, Shanghai, China). Protein concentration was measured using the Bradford method. Equal amounts protein lysates were separated on SDS-PAGE and transferred to polyvinylidene difluoride membranes (Millipore). The membranes were blocked and incubated with primary antibodies against UCP1 (1:1000, Abcam), TPH1 (1:1000; Millipore), β -actin (Sigma-Aldrich) or GAPDH (1:1000; Cell Signaling Technology; Danvers, MA), followed by incubation with HRP-labeled goat anti-rabbit IgG as secondary antibody (1:5000, BOSTER, Wuhan, China). The protein bands were detected by ECL kit (Thermo Fisher Scientific, Rockford, IL) in

ImageQuant LAS 4000 mini (GE Healthcare, Chicago, IL) and quantified using ImageQuant TL 7.0 software (GE Healthcare). Data were showed as the ratio of specific protein to β -actin.

QUANTIFICATION AND STATISTICAL ANALYSIS

All data were presented as means \pm SEM. Because of relatively small sample sizes and often skewed data distribution, we selected the non-parametric Mann-Whitney *U* test for paired datasets and one-way ANOVA with post hoc Bonferroni test was used for comparison among three or more groups to examine statistical significance. $p < 0.05$ was considered as statistically significant. Replicate information is included in the figure legends. In each figure legend, n represents the number of mice used in each indicated group.

Supplementary Material

Refer to Web version on PubMed Central for supplementary material.

ACKNOWLEDGMENTS

This work was supported by projects from the National Natural Science Foundation of China (grants 31471320 and 31671485 to J.L. and 31401204 to B.B.), the Anhui Provincial Natural Science Foundation (grant 1408085QC48 to B.B.), and the National Heart, Lung, and Blood Institute (HL60942, HL123568, and AG058670 to G.-P.S.). Dr. Xian Zhang is supported by American Heart Association postdoctoral fellowship 18POST34050043.

REFERENCES

- Abreu-Vieira G, Fischer AW, Mattsson C, de Jong JM, Shabalina IG, Rydén M, Laurencikiene J, Arner P, Cannon B, Nedergaard J, and Petrovic N (2015). Cidea improves the metabolic profile through expansion of adipose tissue. *Nat. Commun* 6, 7433. [PubMed: 26118629]
- Berglund ED, Liu C, Sohn JW, Liu T, Kim MH, Lee CE, Vianna CR, Williams KW, Xu Y, and Elmquist JK (2013). Serotonin 2C receptors in pro-opiomelanocortin neurons regulate energy and glucose homeostasis. *J. Clin. Invest* 123, 5061–5070. [PubMed: 24177424]
- Boström P, Wu J, Jedrychowski MP, Korde A, Ye L, Lo JC, Rasbach KA, Boström EA, Choi JH, Long JZ, et al. (2012). A PGC1- α -dependent myokine that drives brown-fat-like development of white fat and thermogenesis. *Nature* 481, 463–468. [PubMed: 22237023]
- Brestoff JR, Kim BS, Saenz SA, Stine RR, Monticelli LA, Sonnenberg GF, Thome JJ, Farber DL, Lutfy K, Seale P, and Artis D (2015). Group 2 innate lymphoid cells promote beiging of white adipose tissue and limit obesity. *Nature* 519, 242–246. [PubMed: 25533952]
- Burton OT, Tamayo J, Medina, Stranks AJ, Miller S, Koleoglou KJ, Weinberg EO, and Oettgen HC (2018). IgE promotes type 2 innate lymphoid cells in murine food allergy. *Clin. Exp. Allergy* 48, 288–296. [PubMed: 29247574]
- Camilleri M (2011). LX-1031, a tryptophan 5-hydroxylase inhibitor, and its potential in chronic diarrhea associated with increased serotonin. *Neurogastroenterol. Motil* 23, 193–200. [PubMed: 21159063]
- Caughey GH (2011). Mast cell proteases as protective and inflammatory mediators. *Adv. Exp. Med. Biol* 716, 212–234. [PubMed: 21713659]
- Chlon TM, and Crispino JD (2012). Combinatorial regulation of tissue specification by GATA and FOG factors. *Development* 139, 3905–3916. [PubMed: 23048181]
- Crane JD, Palanivel R, Mottillo EP, Bujak AL, Wang H, Ford RJ, Collins A, Blümer RM, Fullerton MD, Yabut JM, et al. (2015). Inhibiting peripheral serotonin synthesis reduces obesity and metabolic dysfunction by promoting brown adipose tissue thermogenesis. *Nat. Med* 21, 166–172. [PubMed: 25485911]

- Cypess AM, Lehman S, Williams G, Tal I, Rodman D, Goldfine AB, Kuo FC, Palmer EL, Tseng YH, Doria A, et al. (2009). Identification and importance of brown adipose tissue in adult humans. *N. Engl. J. Med* 360, 1509–1517. [PubMed: 19357406]
- Du ZY, Ma T, Lock EJ, Hao Q, Kristiansen K, Frøyland L, and Madsen L (2011). Depot-dependent effects of adipose tissue explants on co-cultured hepatocytes. *PLoS ONE* 6, e20917. [PubMed: 21687689]
- Fabbiano S, Suárez-Zamorano N, Rigo D, Veyrat-Durebex C, Dokic A, Stevanovic, Colin DJ, and Trajkovski M (2016). Caloric Restriction Leads to Browning of White Adipose Tissue through Type 2 Immune Signaling. *Cell Metab* 24, 434–446. [PubMed: 27568549]
- Fisher FM, Kleiner S, Douris N, Fox EC, Mepani RJ, Verdeguer F, Wu J, Kharitonov A, Flier JS, Maratos-Flier E, and Spiegelman BM (2012). FGF21 regulates PGC-1 α and browning of white adipose tissues in adaptive thermogenesis. *Genes Dev* 26, 271–281. [PubMed: 22302939]
- García-Alonso V, Titos E, Alcaraz-Quiles J, Rius B, Lopategi A, López-Vicario C, Jakobsson PJ, Delgado S, Lozano J, and Clária J (2016). Prostaglandin E2 Exerts Multiple Regulatory Actions on Human Obese Adipose Tissue Remodeling, Inflammation, Adaptive Thermogenesis and Lipolysis. *PLoS ONE* 11, e0153751. [PubMed: 27124181]
- Gershon MD, and Ross LL (1966). Location of sites of 5-hydroxytryptamine storage and metabolism by radioautography. *J. Physiol* 186, 477–492. [PubMed: 5298337]
- Ghorbani M, Claus TH, and Himms-Hagen J (1997). Hypertrophy of brown adipocytes in brown and white adipose tissues and reversal of diet-induced obesity in rats treated with a beta3-adrenoceptor agonist. *Biochem. Pharmacol* 54, 121–131. [PubMed: 9296358]
- Gri G, Piconese S, Frossi B, Manfredi V, Merluzzi S, Tripodo C, Viola A, Odom S, Rivera J, Colombo MP, and Pucillo CE (2008). CD4+CD25+ regulatory T cells suppress mast cell degranulation and allergic responses through OX40-OX40L interaction. *Immunity* 29, 771–781. [PubMed: 18993084]
- Gutierrez DA, Muralidhar S, Feyerabend TB, Herzig S, and Rodewald HR (2015). Hematopoietic Kit Deficiency, rather than Lack of Mast Cells, Protects Mice from Obesity and Insulin Resistance. *Cell Metab* 21, 678–691. [PubMed: 25955205]
- Harms M, and Seale P (2013). Brown and beige fat: development, function and therapeutic potential. *Nat. Med* 19, 1252–1263. [PubMed: 24100998]
- He GP, Muise A, Li AW, and Ro HS (1995). A eukaryotic transcriptional repressor with carboxypeptidase activity. *Nature* 378, 92–96. [PubMed: 7477299]
- He B, Bi K, Jia Y, Wang J, Lv C, Liu R, Zhao L, Xu H, Chen X, and Li Q (2013). Rapid analysis of neurotransmitters in rat brain using ultra-fast liquid chromatography and tandem mass spectrometry: application to a comparative study in normal and insomnic rats. *J. Mass Spectrom* 48, 969–978. [PubMed: 23893645]
- Kaisanlahti A, and Glumoff T (2019). Browning of white fat: agents and implications for beige adipose tissue to type 2 diabetes. *J. Physiol. Biochem* 75, 1–10. [PubMed: 30506389]
- Kajimura S, and Saito M (2014). A new era in brown adipose tissue biology: molecular control of brown fat development and energy homeostasis. *Annu. Rev. Physiol* 76, 225–249. [PubMed: 24188710]
- Kajimura S, Spiegelman BM, and Seale P (2015). Brown and Beige Fat: Physiological Roles beyond Heat Generation. *Cell Metab* 22, 546–559. [PubMed: 26445512]
- Kalesnikoff J, and Galli SJ (2008). New developments in mast cell biology. *Nat. Immunol* 9, 1215–1223. [PubMed: 18936782]
- Kalin S, Becker M, Ott VB, Serr I, Hosp F, Mollah MMH, Keipert S, Lamp D, Rohner-Jeanrenaud F, Flynn VK, et al. (2017). A Stat6/Pten Axis Links Regulatory T Cells with Adipose Tissue Function. *Cell Metab* 26, 475–492.e7. [PubMed: 28877454]
- Karlstedt K, Ahman MJ, Anichtchik OV, Soynila S, and Panula P (2003). Expression of the H3 receptor in the developing CNS and brown fat suggests novel roles for histamine. *Mol. Cell. Neurosci* 24, 614–622. [PubMed: 14664812]
- Knudsen JG, Murholm M, Carey AL, Biensø RS, Basse AL, Allen TL, Hidalgo J, Kingwell BA, Febbraio MA, Hansen JB, and Pilegaard H (2014). Role of IL-6 in exercise training- and cold-

induced UCP1 expression in subcutaneous white adipose tissue. *PLoS ONE* 9, e84910. [PubMed: 24416310]

Kohlgruber AC, Gal-Oz ST, LaMarche NM, Shimazaki M, Duquette D, Koay HF, Nguyen HN, Mina AI, Paras T, Tavakkoli A, et al. (2018). $\gamma\delta$ T cells producing interleukin-17A regulate adipose regulatory T cell homeostasis and thermogenesis. *Nat. Immunol* 19, 464–474. [PubMed: 29670241]

Kovanen PT, Nikkilä EA, and Miettinen TA (1975). Regulation of cholesterol synthesis and storage in fat cells. *J. Lipid Res* 16, 211–223. [PubMed: 1127358]

Krause BR, and Hartman AD (1984). Adipose tissue and cholesterol metabolism. *J. Lipid Res* 25, 97–110. [PubMed: 6368715]

Kumar RK, Chapple CC, and Hunter N (1999). Improved double immunofluorescence for confocal laser scanning microscopy. *J. Histochem. Cytochem* 47, 1213–1218. [PubMed: 10449542]

Laporta J, Keil KP, Vezina CM, and Hernandez LL (2014). Peripheral serotonin regulates maternal calcium trafficking in mammary epithelial cells during lactation in mice. *PLoS ONE* 9, e110190. [PubMed: 25299122]

Lee YH, Petkova AP, Mottillo EP, and Granneman JG (2012). In vivo identification of bipotential adipocyte progenitors recruited by β 3-adrenoceptor activation and high-fat feeding. *Cell Metab* 15, 480–491. [PubMed: 22482730]

Lee MW, Odegaard JI, Mukundan L, Qiu Y, Molofsky AB, Nussbaum JC, Yun K, Locksley RM, and Chawla A (2015). Activated type 2 innate lymphoid cells regulate beige fat biogenesis. *Cell* 160, 74–87. [PubMed: 25543153]

Lim S, Honek J, Xue Y, Seki T, Cao Z, Andersson P, Yang X, Hosaka K, and Cao Y (2012). Cold-induced activation of brown adipose tissue and adipose angiogenesis in mice. *Nat. Protoc* 7, 606–615. [PubMed: 22383039]

Liu J, Divoux A, Sun J, Zhang J, Clément K, Glickman JN, Sukhova GK, Wolters PJ, Du J, Gorgun CZ, et al. (2009). Genetic deficiency and pharmacological stabilization of mast cells reduce diet-induced obesity and diabetes in mice. *Nat. Med* 15, 940–945. [PubMed: 19633655]

Loyd C, and Obici S (2014). Brown fat fuel use and regulation of energy homeostasis. *Curr. Opin. Clin. Nutr. Metab. Care* 17, 368–372. [PubMed: 24839950]

Lynch L, Hogan AE, Duquette D, Lester C, Banks A, LeClair K, Cohen DE, Ghosh A, Lu B, Corrigan M, et al. (2016). iNKT Cells Induce FGF21 for Thermogenesis and Are Required for Maximal Weight Loss in GLP1 Therapy. *Cell Metab* 24, 510–519. [PubMed: 27593966]

Clair J, Mallen-St, Pham CT, Villalta SA, Caughey GH, and Wolters PJ (2004). Mast cell dipeptidyl peptidase I mediates survival from sepsis. *J. Clin. Invest* 113, 628–634. [PubMed: 14966572]

Mössenböck K, Vegiopoulos A, Rose AJ, Sijmonsma TP, Herzig S, and Schafmeier T (2014). Browning of white adipose tissue uncouples glucose uptake from insulin signaling. *PLoS ONE* 9, e110428. [PubMed: 25313899]

Nguyen KD, Qiu Y, Cui X, Goh YP, Mwangi J, David T, Mukundan L, Brombacher F, Locksley RM, and Chawla A (2011). Alternatively activated macrophages produce catecholamines to sustain adaptive thermogenesis. *Nature* 480, 104–108. [PubMed: 22101429]

Nigrovic PA, Gray DH, Jones T, Hallgren J, Kuo FC, Chaletzky B, Gurish M, Mathis D, Benoist C, and Lee DM (2008). Genetic inversion in mast cell-deficient (Wsh) mice interrupts corin and manifests as hematopoietic and cardiac aberrancy. *Am. J. Pathol* 173, 1693–1701. [PubMed: 18988802]

Oh CM, Namkung J, Go Y, Shong KE, Kim K, Kim H, Park BY, Lee HW, Jeon YH, Song J, et al. (2015). Regulation of systemic energy homeostasis by serotonin in adipose tissues. *Nat. Commun* 6, 6794. [PubMed: 25864946]

Ohno H, Shinoda K, Spiegelman BM, and Kajimura S (2012). PPAR γ agonists induce a white-to-brown fat conversion through stabilization of PRDM16 protein. *Cell Metab* 15, 395–404. [PubMed: 22405074]

Piconese S, Gri G, Tripodo C, Musio S, Gorzanelli A, Frossi B, Pedotti R, Pucillo CE, and Colombo MP (2009). Mast cells counteract regulatory T-cell suppression through interleukin-6 and OX40/OX40L axis toward Th17-cell differentiation. *Blood* 114, 2639–2648. [PubMed: 19643985]

- Qiu Y, Nguyen KD, Odegaard JI, Cui X, Tian X, Locksley RM, Palmiter RD, and Chawla A (2014). Eosinophils and type 2 cytokine signaling in macrophages orchestrate development of functional beige fat. *Cell* 157, 1292–1308. [PubMed: 24906148]
- Rao RR, Long JZ, White JP, Svensson KJ, Lou J, Lokurkar I, Jedrychowski MP, Ruas JL, Wrann CD, Lo JC, et al. (2014). Meteorin-like is a hormone that regulates immune-adipose interactions to increase beige fat thermogenesis. *Cell* 157, 1279–1291. [PubMed: 24906147]
- Rodewald HR, and Feyerabend TB (2012). Widespread immunological functions of mast cells: fact or fiction? *Immunity* 37, 13–24. [PubMed: 22840840]
- Rosen ED, and Spiegelman BM (2014). What we talk about when we talk about fat. *Cell* 156, 20–44. [PubMed: 24439368]
- Sakata T, Kang M, Kurokawa M, and Yoshimatsu H (1995). Hypothalamic neuronal histamine modulates adaptive behavior and thermogenesis in response to endogenous pyrogen. *Obes. Res* 3 (Suppl 5), 707S–712S. [PubMed: 8653552]
- Seale P, Bjork B, Yang W, Kajimura S, Chin S, Kuang S, Scimé A, Devarakonda S, Conroe HM, Erdjument-Bromage H, et al. (2008). PRDM16 controls a brown fat/skeletal muscle switch. *Nature* 454, 961–967. [PubMed: 18719582]
- Shan T, Liang X, Bi P, Zhang P, Liu W, and Kuang S (2013). Distinct populations of adipogenic and myogenic Myf5-lineage progenitors in white adipose tissues. *J. Lipid Res* 54, 2214–2224. [PubMed: 23740968]
- Stanford KI, Middelbeek RJ, Townsend KL, An D, Nygaard EB, Hitchcox KM, Markan KR, Nakano K, Hirshman MF, Tseng YH, and Good-year LJ (2013). Brown adipose tissue regulates glucose homeostasis and insulin sensitivity. *J. Clin. Invest* 123, 215–223. [PubMed: 23221344]
- Stock K, and Westermann EO (1963). Concentration of Norepinephrine, Serotonin, and Histamine, and of Amine-Metabolizing Enzymes in Mammalian Adipose Tissue. *J. Lipid Res* 4, 297–304. [PubMed: 14168167]
- Tecott LH (2007). Serotonin and the orchestration of energy balance. *Cell Metab* 6, 352–361. [PubMed: 17983581]
- Thevenot PT, Baker DW, Weng H, Sun MW, and Tang L (2011). The pivotal role of fibrocytes and mast cells in mediating fibrotic reactions to biomaterials. *Biomaterials* 32, 8394–8403. [PubMed: 21864899]
- Uldry M, Yang W, St-Pierre J, Lin J, Seale P, and Spiegelman BM (2006). Complementary action of the PGC-1 coactivators in mitochondrial biogenesis and brown fat differentiation. *Cell Metab* 3, 333–341. [PubMed: 16679291]
- Virtanen KA, Lidell ME, Orava J, Heglind M, Westergren R, Niemi T, Taittonen M, Laine J, Savisto NJ, Enerbäck S, and Nuutila P (2009). Functional brown adipose tissue in healthy adults. *N. Engl. J. Med* 360, 1518–1525. [PubMed: 19357407]
- Wang J, Cheng X, Xiang MX, Alanne-Kinnunen M, Wang JA, Chen H, He A, Sun X, Lin Y, Tang TT, et al. (2011). IgE stimulates human and mouse arterial cell apoptosis and cytokine expression and promotes atherogenesis in Apoe^{-/-} mice. *J. Clin. Invest* 121, 3564–3577. [PubMed: 21821913]
- Watanabe M, Houten SM, Matakai C, Christoffolete MA, Kim BW, Sato H, Messaddeq N, Harney JW, Ezaki O, Kodama T, et al. (2006). Bile acids induce energy expenditure by promoting intracellular thyroid hormone activation. *Nature* 439, 484–489. [PubMed: 16400329]
- Wolters PJ, Clair J, Mallen-St, Lewis CC, Villalta SA, Baluk P, Erle DJ, and Caughey GH (2005). Tissue-selective mast cell reconstitution and differential lung gene expression in mast cell-deficient Kit(W-sh)/Kit(W-sh) sash mice. *Clin. Exp. Allergy* 35, 82–88. [PubMed: 15649271]
- Wu Z, Puigserver P, Andersson U, Zhang C, Adelmant G, Mootha V, Troy A, Cinti S, Lowell B, Scarpulla RC, and Spiegelman BM (1999). Mechanisms controlling mitochondrial biogenesis and respiration through the thermogenic coactivator PGC-1. *Cell* 98, 115–124. [PubMed: 10412986]
- Wu J, Boström P, Sparks LM, Ye L, Choi JH, Giang AH, Khandekar M, Virtanen KA, Nuutila P, Schaart G, et al. (2012). Beige adipocytes are a distinct type of thermogenic fat cell in mouse and human. *Cell* 150, 366–376. [PubMed: 22796012]
- Würden S, and Homberg U (1993). A simple method for immunofluorescent double staining with primary antisera from the same species. *J. Histochem. Cytochem* 41, 627–630. [PubMed: 8450202]

- Yadav H, Quijano C, Kamaraju AK, Gavrilova O, Malek R, Chen W, Zerfas P, Zhigang D, Wright EC, Stuelten C, et al. (2011). Protection from obesity and diabetes by blockade of TGF- β /Smad3 signaling. *Cell Metab* 14, 67–79. [PubMed: 21723505]
- Zhang Z, Zhang H, Li B, Meng X, Wang J, Zhang Y, Yao S, Ma Q, Jin L, Yang J, et al. (2014). Berberine activates thermogenesis in white and brown adipose tissue. *Nat. Commun* 5, 5493. [PubMed: 25423280]
- Zhang X, Zhang QX, Wang X, Zhang L, Qu W, Bao B, Liu CA, and Liu J (2016). Dietary luteolin activates browning and thermogenesis in mice through an AMPK/PGC1 α pathway-mediated mechanism. *Int. J. Obes* 40, 1841–1849.
- Zhang X, Huang Q, Wang X, Deng Z, Li J, Yan X, Jauhainen M, Metso J, Libby P, Liu J, and Shi GP (2019). Dietary cholesterol is essential to mast cell activation and associated obesity and diabetes in mice. *Biochim. Biophys. Acta Mol. Basis Dis* 1865, 1690–1700. [PubMed: 30978390]
- Zhou Y, Yu X, Chen H, Sjöberg S, Roux J, Zhang L, Ivoulsou AH, Ben-said F, Liu CL, Liu J, et al. (2015). Leptin Deficiency Shifts Mast Cells toward Anti-Inflammatory Actions and Protects Mice from Obesity and Diabetes by Polarizing M2 Macrophages. *Cell Metab* 22, 1045–1058. [PubMed: 26481668]

Highlights

- Mast cell inactivation increases mouse systemic thermogenesis and energy expenditure
- Mast cell inactivation enhances SAT thermogenic gene expression and adipocyte browning
- Mast cell inactivation increases SAT PDGFR α ⁺ adipocyte precursor proliferation
- Mast cell serotonin blocks adipocyte browning and energy expenditure

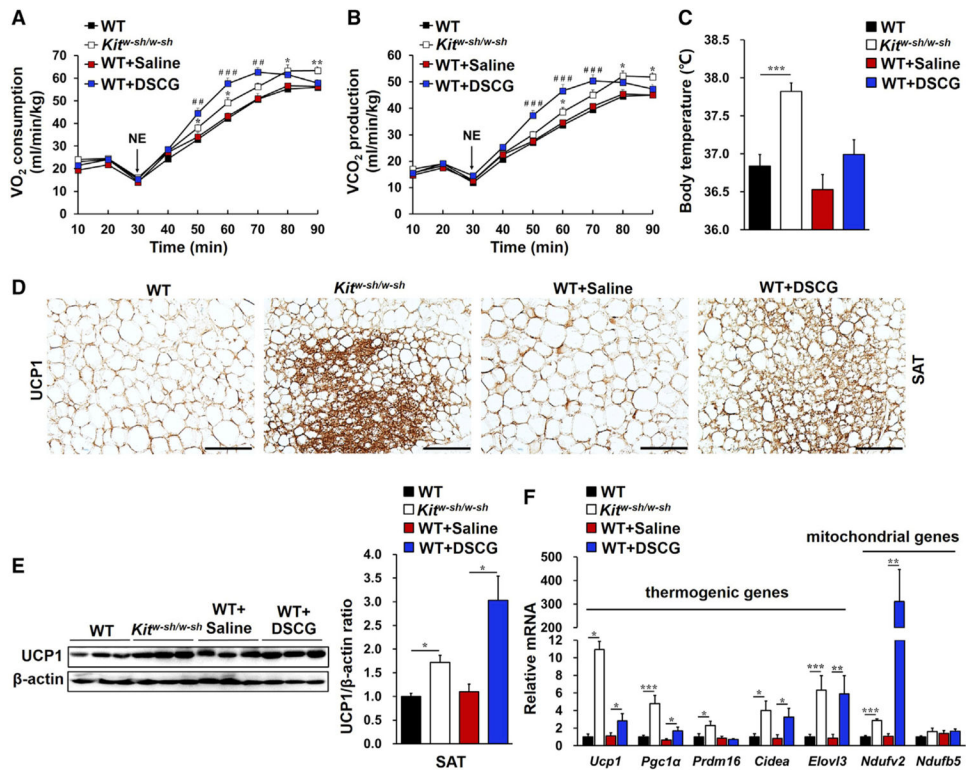


Figure 1. MCs Controlled Systemic Energy Expenditure and SAT Thermogenesis and Browning in Mice on a Chow Diet

(A and B) NE-stimulated mouse metabolic rate, including oxygen consumption (VO_2 ; A) and carbon dioxide production (VCO_2 ; B) in WT mice (n = 13), *Kit^{w-sh/w-sh}* mice (n = 13), WT mice receiving saline (WT+Saline, n = 13) or DSCG (WT+DSCG, n = 16) intraperitoneal (i.p.) injections.

(C) Core body temperatures for the indicated groups of mice.

(D) UCP1 immunostaining of representative SAT sections (n = 8 per group); scale bars, 100 μ m.

(E) Immunoblot analysis and quantification of UCP1 relative to β -actin in SAT (n = 6 per group).

(F) Real-time PCR analysis of thermogenic and mitochondrial genes in SAT (n = 8~13 per group).

Data are mean \pm SEM. *p < 0.05, **p < 0.01, ***p < 0.001.

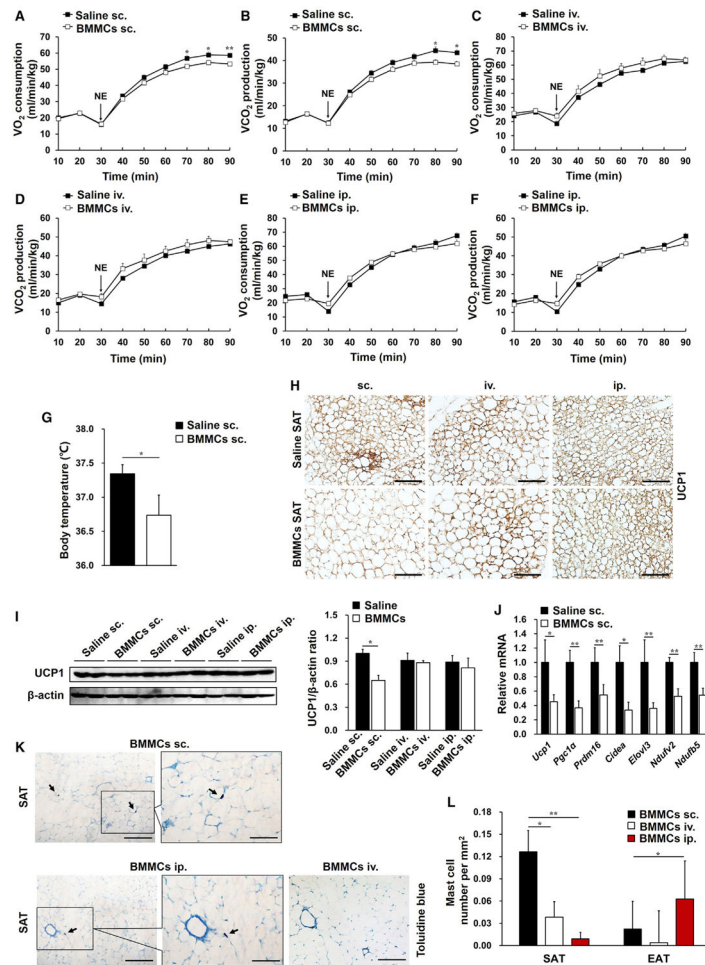


Figure 2. MC Reconstitution into SAT Reduced Systemic Energy Metabolism and SAT Browning (A–F) NE-stimulated VO_2 (A, C, and E) and VCO_2 (B, D, and F) in *Kit^{w-sh/w-sh}* mice 6 weeks after receiving subcutaneous (s.c.) (A and B), intravenous (i.v.) (C and D), or i.p. (E and F) injections of saline or BMMCs from WT mice. $n = 8–14$ per cohort. (G) Core body temperature of *Kit^{w-sh/w-sh}* mice receiving s.c. injections of saline or BMMCs ($n = 8–12$ per group). (H) UCP1 immunostaining ($n = 8$ per group). (I) UCP1 immunoblot and quantification relative to β -actin in SAT after different approaches of BMMC adoptive transfer ($n = 6$ per group). (J) Real-time PCR analysis of thermogenic and mitochondrial genes in SAT from mice receiving s.c. injection of saline or BMMCs ($n = 12$ per group). (K) Toluidine blue staining for MCs (arrows) in representative SAT sections after BMMC adoptive transfer ($n = 8$ per group). (L) MC number quantification in SAT and EAT from *Kit^{w-sh/w-sh}* mice receiving s.c., i.v., and i.p. BMMC adoptive transfers ($n = 8–14$ per group). Scale bars, 100 μ m; inset scale bars, 50 μ m. Data are mean \pm SEM. * $p < 0.05$, ** $p < 0.01$.

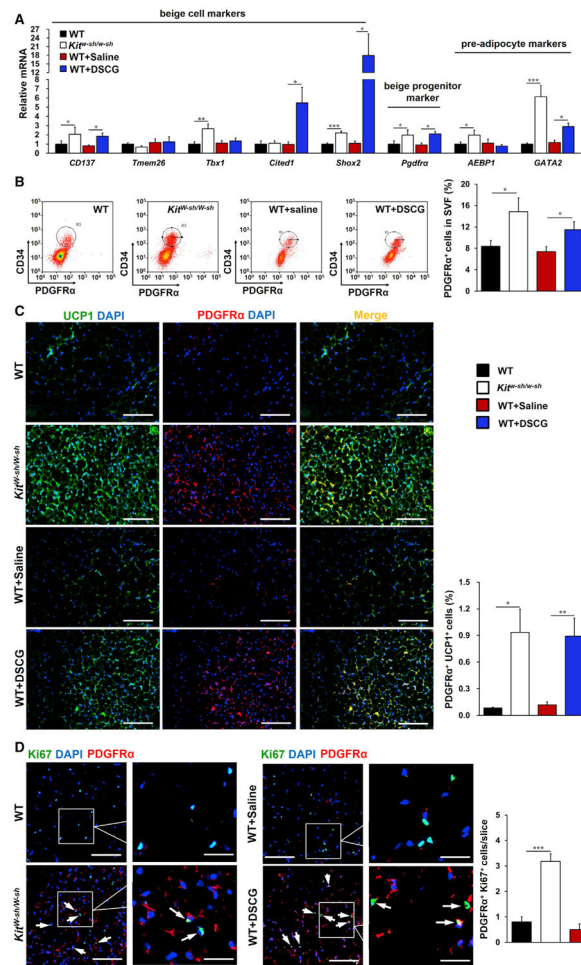


Figure 3. MCs Inhibited SAT PDGFR α ⁺ Beige Progenitor Cell Proliferation and Browning
 (A) Real-time PCR analysis of beige cell markers, beige progenitor marker *Pdgfra*, and pre-adipocyte markers in SAT from the indicated groups of mice (n = 8–13 per group).
 (B) FACS analysis of PDGFR α ⁺ cells in SAT (as defined by CD34⁺ PDGFR α ⁺). n = 8~10 per group.
 (C) Immunofluorescent double staining of PDGFR α ⁺ (red) and UCP1⁺ (green) double-positive cells.
 (D) Immunofluorescent double staining of PDGFR α ⁺ (red) and Ki67⁺ (green) double-positive cells in SAT, with nuclei counterstained with DAPI (blue) (n = 8 per group).
 Scale bars, 100 μ m; inset scale bars, 25 μ m. Representative images in (B)–(D) are shown on the left.
 Data are mean \pm SEM. *p < 0.05, **p < 0.01, ***p < 0.001.

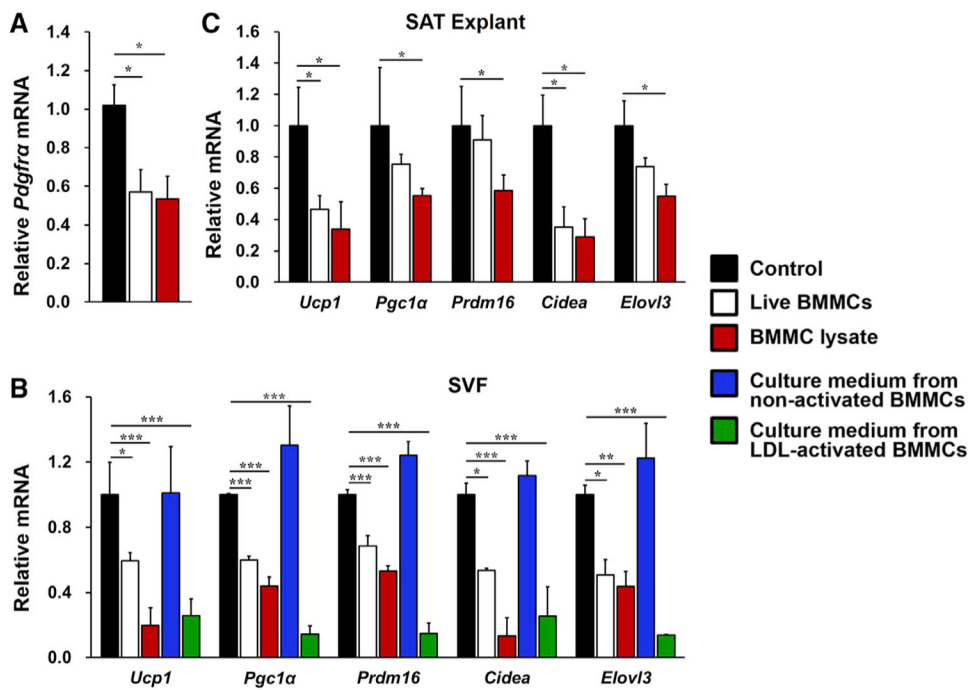
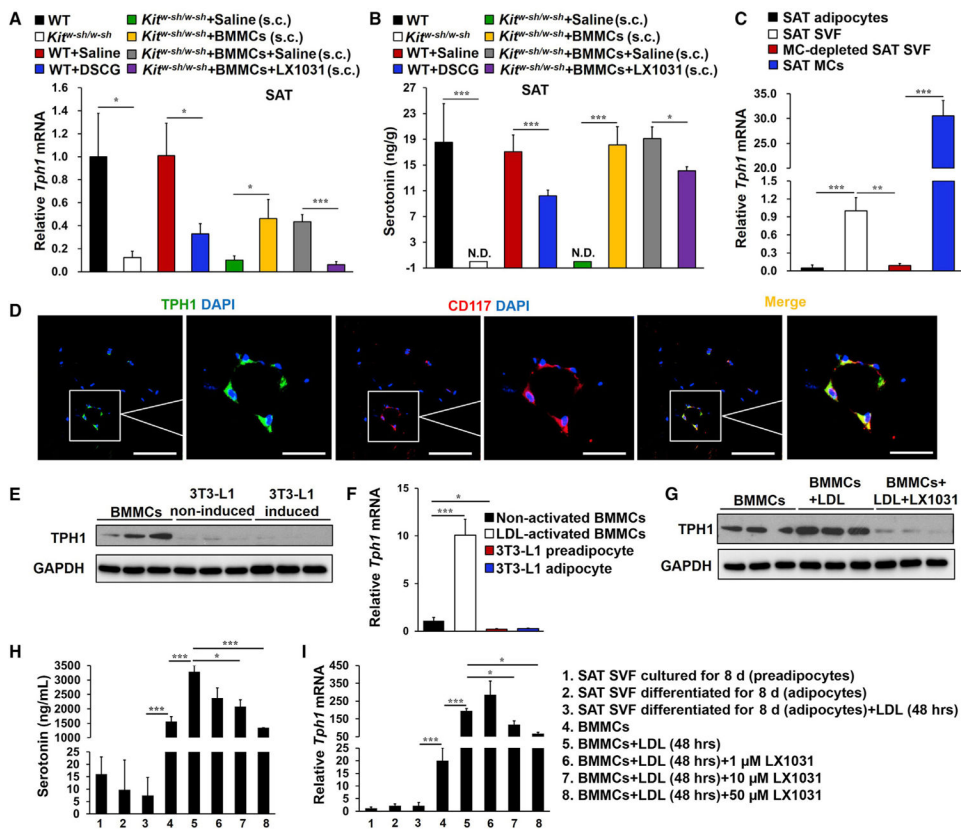


Figure 4. MCs Inhibited SAT PDGFR α Expression and Browning Differentiation in SAT SVF (A–C) Real-time PCR determined relative mRNA levels of (A) *Pdgfra* in SVF preadipocytes from WT mouse SAT after 6 days of culture without or with live BMMCs or BMMC lysates (n = 4 per group); (B) the thermogenic and mitochondrial genes in the SVF from WT mouse SAT after 8 days of culture in browning differentiation cocktail without or with live BMMCs, BMMC lysates, and culture medium from non-activated or LDL-activated BMMCs (n = 4 per group); and (C) thermogenic genes in MC-deficient *Kit^{w-sh/w-sh}* mouse SAT explants after 24 h of culture without or with live BMMCs or BMMC lysates (n = 4 per group). Data are mean \pm SEM, *p < 0.05, **p < 0.01, ***p < 0.001.



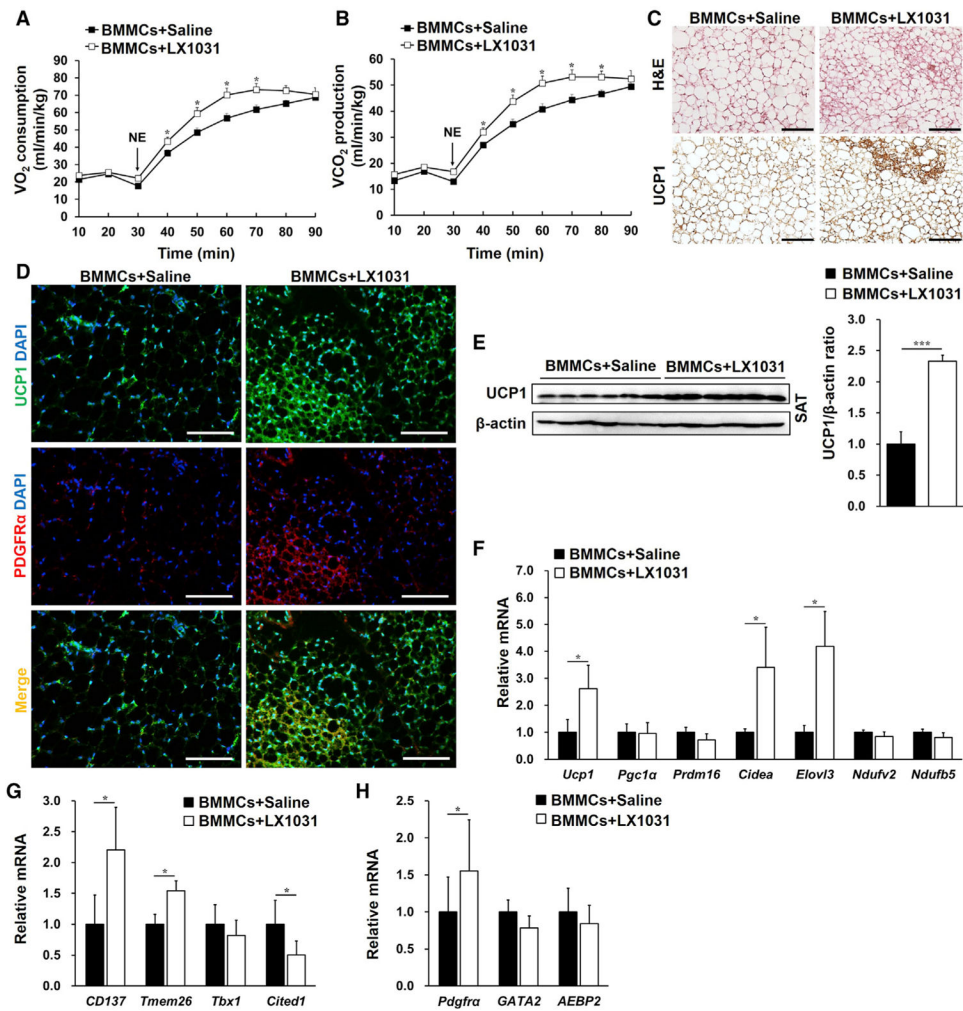


Figure 6. MC-Derived Serotonin Inhibited Systemic Energy Expenditure and the SAT Thermogenic Program

(A–H) NE-stimulated VO_2 (A) and VCO_2 (B); H&E staining and UCP1 immunostaining (C); PDGFR α (red) and UCP1 (green) immunofluorescent double staining (D); immunoblot analysis of UCP1 and quantification relative to β -actin (E); and real-time PCR analysis of thermogenic and mitochondrial genes (F), beige cell markers (G), the beige progenitor marker *Pdgfra*, and pre-adipocyte markers (H) in SAT from *Kit^{w-sh/w-sh}* mice receiving WT BMMCs s.c. and daily s.c. injections of saline or LX1031 for 6 weeks (n = 8 per group). Scale bars, 100 μ m.

Data are mean \pm SEM. *p < 0.05, **p < 0.01, ***p < 0.001.

KEY RESOURCES TABLE

REAGENT or RESOURCE	SOURCE	IDENTIFIER
Antibodies		
Anti-mouse PDGFR α (CD140a)-APC	BioLegend	Cat# 135907; RRID:AB_2043969
Anti-CD34-FITC	eBioscience	Cat# 11-0341-85; RRID:AB_465022
Anti-CD45-PE	eBioscience	Cat# 12-0451-83; RRID:AB_465669
Anti-CD117-APC	eBioscience	Cat# 17-1171-82; RRID:AB_469430
Anti-FCeR1-PE-CY7	eBioscience	Cat# 25-5898-82; RRID:AB_2573493
Anti-mouse PDGFR α	R&D	Cat# AF1062; RRID:AB_2236897
Anti-mouse CD117	ebioscience	Cat# 14-1171-85; RRID:AB_467434
Anti-mouse UCP1	Abcam	Cat# 10983; RRID:AB_2241462
Anti-TPH1	Millipore	Cat# AB15570; RRID:AB_877305
Anti-Ki67	Novus	Cat# NB600-1209; RRID:AB_10001641
Anti- β -actin	Sigma-Aldrich	Cat# A1978; RRID:AB_476692
Anti-GAPDH	Cell Signaling Technology	Cat# 2118; RRID:AB_561053
Chemicals, Peptides, and Recombinant Proteins		
High-fat diet	Research Diets	Cat# D12492
Control chow diet	Research Diets	Cat# D12450B
Norepinephrine	Sigma-Aldrich	Cat# A7257
Oil-red O	Sigma	Cat# O0625
LDL-c	Lee Biosolutions	Cat# 360-10
Type II collagenase	Worthington	Cat# LS004177
RPMI 1640	GIBCO	Cat# 61870-036
DMEM	GIBCO	Cat# 10566-016
LX1031	Medchem Express	Cat# HY-13041
Recombinant IL-3	PeproTech	Cat# 213-13
Recombinant stem cell factor	PeproTech	Cat# 250-03
3,3',5-triiodo-L-thyronine (T3)	Sigma-Aldrich	Cat# T2877
Isobutylmethylxanthine	Sigma-Aldrich	Cat# I7018
Dexamethasone	Sigma-Aldrich	Cat# D4902
Indomethacin	Sigma-Aldrich	Cat# I7378
Rosiglitazone	Sigma-Aldrich	Cat# R2408
Insulin	Sigma-Aldrich	Cat# 91077C
Haematoxylin	Sigma-Aldrich	Cat# GHS316
Eosin	Sigma-Aldrich	Cat# HT110116
Toluidine blue	Sigma-Aldrich	Cat# 89640
DAPI	Sangon Biotech	Cat# E607303
SYBR green dye	TAKARA	Cat# DRR081A
Critical Commercial Assays		

REAGENT or RESOURCE	SOURCE	IDENTIFIER
Serotonin	LDN	Cat# BA E-8900
Experimental Models: Cell Lines		
3T3-L1	ATCC	Cat# CL-173
Experimental Models: Organisms/Strains		
Wild-type (C57BL/6J)	Vital River Laboratory Animal Technology Co. Ltd. (Beijing, China)	Cat# 213
<i>Ki^{w-sh/w-sh}</i> (C57BL/6J) B6.Cg-KitW-sh/HNhrJaeBsmJ	Jackson Laboratory (purchased during last 7 years and bred at Hefei)	Cat# 030764
<i>Tph1^{-/-}</i> mice (C57BL/6J)	University of Wisconsin-Madison	N/A
Software and Algorithms		
Image-Pro plus 6.0	Media Cybernetics, Inc.	http://www.mediacy.com/imageproplus
Kaluza Analysis	Beckman Coulter	https://en.freedownloadmanager.org/Windows-PC/Kaluza-Analysis.html